Pergamon

Geochimica et Cosmochimica Acta, Vol. 68, No. 20, pp. 4237-4248, 2004

0016-7037/04 $30.00 + .00

doi:10.1016/j.gca.2004.04.008

A preferred method for the determination of bulk compositions of coarse-grained refractory inclusions and some implications of the results

S. B. SIMON[1,*] and L. GROSSMAN[1,2]

[1]Dept. of the Geophysical Sciences, 5734 S. Ellis Ave., The University of Chicago, Chicago, IL 60637 USA
[2]Enrico Fermi Institute, 5640 S. Ellis Ave., The University of Chicago, Chicago, IL 60637 USA

(*Received December* 12, 2003; *accepted in revised form April* 21, 2004)

Abstract—Analyses of coarse-grained refractory inclusions typically do not have the solar CaO/Al_2O_3 ratio, probably reflecting nonrepresentative sampling of them in the laboratory. Many previous studies, especially those done by instrumental neutron activation analysis (INAA), were based on very small amounts of material removed from those restricted portions of inclusions that happened to be exposed on surfaces of bulk meteorite samples. Here, we address the sampling problem by studying thin sections of large inclusions, and by analyzing much larger aliquots of powders of these inclusions by INAA than has typically been done in the past. These results do show convergence toward the solar CaO/Al_2O_3 ratio of 0.792. The bulk compositions of 15 coarse-grained inclusions determined by INAA of samples >2 mg have an average CaO/Al_2O_3 ratio of 0.80 ± 0.18. When bulk compositions are obtained by modal recombination based on analysis of thin sections with cross-sections of entire, large, unbroken inclusions, the average of 11 samples (0.79 ± 0.15) also matches the solar value. Among those analyzed by INAA and by modal recombination, there were no inclusions for which both techniques agreed on a CaO/Al_2O_3 ratio deviating by $>\sim$15% from the solar value. These results suggest that: individual inclusions may have the solar CaO/Al_2O_3 ratio; departures from this value are due to sample heterogeneity and nonrepresentative sampling in the laboratory; and it is therefore valid to correct compositions to this value. We present a method for doing so by mathematical addition or subtraction of melilite, spinel, or pyroxene. This yields a set of multiple, usually slightly different, corrected compositions for each inclusion. The best estimate of the bulk composition of an inclusion is the average of these corrected compositions, which simultaneously accounts for errors in sampling of all major phases. Results show that Type B2 inclusions tend to be more SiO_2-rich and have higher normative Anorthite/Gehlenite component ratios than Type B1s. The inclusion bulk compositions lie in a field that can result from evaporation at 1700–2000K of CMAS liquids with solar CaO/Al_2O_3, but with a wide range of initial MgO (30–60 wt%) and SiO_2 (15–50 wt%) contents.

1. INTRODUCTION

There are two major types of coarse-grained refractory inclusions found in the CV3 carbonaceous chondrites, such as Allende: those that are very melilite-rich, with minor perovskite and hibonite (Type As), and those that contain major amounts of clinopyroxene in addition to melilite and minor amounts of anorthite (Type Bs). Both types also contain Mg-Al spinel. Because these phases are predicted to condense at high temperatures from a gas of solar composition, it has been suggested (e.g., Grossman, 1972) that these inclusions represent some of the earliest condensates from the nebula or melts of early condensate assemblages. It has also been known for a long time, however, that inclusion bulk compositions differ from those of equilibrium condensate assemblages. Thermodynamic calculations (Grossman, 1972; Yoneda and Grossman, 1995) show that the bulk compositions of condensate assemblages change with decreasing temperature, and this sequence of compositions forms a trend or trajectory. Inclusion bulk compositions tend to plot near condensate trajectories but are displaced from them toward relatively MgO-poor compositions (e.g., Stolper, 1982; Grossman et al., 2000; Lin and Kimura, 2003). The Mg and Si isotopic compositions of compact Type A and Type B refractory inclusions commonly show enrichments in the heavy isotopes, suggesting that significant amounts were lost by evaporation (Clayton et al., 1988). Calculations show that the bulk chemical compositions of refractory inclusions could have been derived by partial evaporation of these elements from melts of high-temperature condensate assemblages into an H_2-rich gas (Grossman et al., 2000; 2002). There are, however, few inclusions for which both bulk chemical and bulk Mg and Si isotopic data exist, so direct evidence of this process remains elusive. This work is the first step in an attempt to solve this problem by presenting a method for recognizing and obtaining accurate bulk chemical compositions for inclusions from CV3 chondrites. The next steps will be to obtain Mg and Si isotopic data for the inclusions and to derive their original, preevaporation compositions.

Thermodynamic calculations (e.g., Grossman, 1972; Yoneda and Grossman, 1995) show that early in the solar nebular condensation sequence, CaO and Al_2O_3 condensed into hibonite, perovskite and gehlenite, and by the temperature at which hibonite disappeared, Ca and Al were totally condensed. With the maximum temperatures of reheating constrained to be within several tens of degrees of the temperature of melilite crystallization (Stolper and Paque, 1986), calculations and experiments (Grossman et al., 2000) show that neither CaO nor Al_2O_3 would have evaporated during any subsequent reheating or remelting experienced by CAIs. The lack of Ca isotopic

* Author to whom correspondence should be addressed (sbs8@midway.uchicago.edu).

fractionation in CAIs (Niederer and Papanastassiou, 1984) is consistent with this result. If we assume that the inclusions formed from representative assemblages of precursor phases, and that neither oxide was lost or gained during secondary alteration, then the true bulk compositions of melilite-bearing, hibonite-free inclusions should have the solar CaO/Al_2O_3 ratio of 0.792 (Anders and Grevesse, 1989).

Published compositions of refractory inclusions have wide ranges of CaO/Al_2O_3 ratios, however. Grossman et al. (2000), starting with bulk compositions of a suite of hibonite-free, coarse-grained inclusions taken from the literature, mathematically added (or subtracted) the amount of stoichiometric spinel to (or from) each that was necessary to yield the solar CaO/Al_2O_3 ratio. They found that the resulting compositions much more closely approximated compositions of equilibrium condensate assemblages in terms of their CaO, MgO, Al_2O_3 and SiO_2 (CMAS) contents. Scatter of the data about several possible condensation trajectories was greatly reduced, and better fits to the condensation trajectories were obtained, even for oxides not present in spinel. The results of the Grossman et al. (2000) study suggest that the true bulk compositions of Types A and B CAIs have the solar CaO/Al_2O_3 ratio and that analyses with deviations from this value reflect nonrepresentative sampling in the laboratory. Grossman et al. (2000) also used thermodynamic calculations to show that evaporative loss of Mg and Si from equilibrium condensates could account for the displacement of CAI bulk compositions from a trajectory of condensate compositions. These losses would not affect the CaO/Al_2O_3 ratios of the inclusions. One of the goals of the present study is to investigate further whether or not hibonite-free, coarse-grained refractory inclusions have the solar CaO/Al_2O_3 ratio, and therefore whether or not the above assumptions are valid. We have addressed this issue by sampling large inclusions as representatively as possible and applying two analytical methods to the samples.

In addition, the Type B inclusions are subdivided into B1s, which have nearly monomineralic melilite mantles enclosing pyroxene-rich cores, and B2s, which have much more uniform distributions of phases. At the outset of the present study, we found that there are very few detailed mineral chemical data available for Type B2 inclusions. Much of what is known about Type B inclusions comes from studies of Type B1 inclusions, and from experiments on analogs of B1 bulk compositions. Previous analyses of Type B inclusions (e.g., Wark and Lovering, 1982) suggest that Type B2 inclusions tend to be more SiO_2-rich than Type B1s. Therefore, inferences about the formation of CAIs that are based on studies of Type B1 compositions should not be routinely extended to Type B2s. Having accurate bulk compositions available will improve our understanding of the formation of both types of inclusions. In this paper, we compare methods of bulk composition determination, present an argument for correction of bulk compositions to the solar CaO/Al_2O_3 ratio and a method for doing so, and discuss some of the systematics observed in the results.

2. EXPERIMENTAL METHODS

2.1. Sampling

As discussed previously (Grossman et al., 2000), accurate determination of bulk chemical compositions of refractory inclusions is fraught with difficulties primarily related to sample heterogeneity and the small and/or nonrepresentative samples typically used for this purpose. For example, a 1 cm-diameter inclusion weighs 1.75 g, but a bulk chemical composition obtained by modal recombination of an equatorial, 30 μm-thick, thin section of it would be based on only 8 mg, or 0.46%, of the sample. Similarly, a bulk composition obtained by instrumental neutron activation analysis (INAA) of a 3 mg fraction of it would be based on only 0.17% of the sample, and most INAA data are based on much smaller samples. In addition, in many cases in the past a thin section would be made from one end of an inclusion while the opposite side was sampled for INAA, so that neither sampled a large, representative cross-section of the inclusion. Material was not always uniformly excavated from exposed surfaces, as sampling for INAA sometimes favored cracked or friable regions. Another problem is that the outermost edges of inclusions often must be undersampled to avoid contamination with matrix.

The inclusions employed in this study were large enough that, in several cases, multiple thin sections could be prepared from one portion and relatively large quantities of material excavated from the remainder. The excavated material from each inclusion was ground into a homogeneous powder (weights ranged from 5–200 mg, but most were ~40 mg) which was divided into separate aliquots for determination of major and some minor elements by INAA; Mg isotopic analysis; O and Si isotopic analysis; and, in some cases, U-Pb geochronologic investigation (Amelin et al., 2002). Though the thin sections are smaller by mass than most of the samples we used for INAA, the rim-to-rim sections we used may be more representative, for the reasons given above.

2.2. Analysis

Na, Mg, Al, Ca, Ti, V and Mn abundances were determined by INAA in a short irradiation using a pneumatic transfer system, and Fe in a long irradiation, at the University of Missouri Research Reactor in each of 6 inclusions from Efremovka, 5 from Allende and one from Leoville. SiO_2 was obtained by difference. Standards used were SRM-688 (basalt) and PCC-1 (peridotite). In the short irradiation, samples and standards were irradiated for two minutes in the first row of the graphite reflector at a flux of 8×10^{13} n/cm^2/s, allowed to decay for 20 min, and then counted for 10 min. The distance between the samples and detector was ~25 cm. For the long irradiation the samples were exposed to a flux of 5×10^{13} n/cm^2/s for 24 h and allowed to cool for seven days before counting. The distance between the samples and detector was ~15 cm. Corrections for fast neutron reactions on Al to produce Mg, $^{27}Al(n,p)^{27}Mg$, were made according to the method of Glascock et al. (1985). Uncertainties due to counting statistics and standardization were always $\leq$0.9% of the amounts present for CaO and MgO, and $\leq$0.6% for Al_2O_3.

Bulk compositions were also determined from thin sections by modal recombination. Backscattered electron images were obtained with a JEOL JSM-5800LV scanning electron microscope. Quantitative wavelength-dispersive analyses were obtained with a Cameca SX-50 electron microprobe operated at 15 kV with a beam current of 50 nA. Regularly-spaced, linear traverses were conducted across the inclusions, from rim to rim, to create grids covering the inclusions. Along the traverse paths, analysis points were 15–25 μm apart, and an average of 2140 wavelength-dispersive analyses were collected per thin section for CaO, MgO, Al_2O_3, SiO_2 and TiO_2 (CMAST). The analysis routine required ~45 s per spot, with detection limits for trace components of 0.025 wt.% TiO_2 in melilite and spinel, and 0.12 wt.% SiO_2 and CaO in spinel. Data were reduced via the modified ZAF correction procedure PAP (Pouchou and Pichoir, 1984). Analyses with totals between 97 and 102% were checked for stoichiometry and identified as either melilite, pyroxene [the Al-, Ti-rich variety termed "fassaite" by Dowty and Clark (1973)], anorthite or spinel; analyses of secondary alteration products (mostly grossular and monticellite) and of contacts between grains having good totals were averaged together as a mixed-phase component. From these analyses we obtained average phase compositions for each inclusion. Analyses with totals from 90 to 97% were also identified mineralogically and included in the calculation of phase proportions, but not in the determination of average phase compositions. The relative abundances of analyses of each phase in a given inclusion are assumed to be directly proportional to their areal and

Table 1. Bulk chemical compositions of refractory inclusions determined by INAA (in wt% unless otherwise noted).

Sample	TS67	TS65	Golfball	3537-2	TS33	TS32	E13	E56	E55	E62	E49	E107
[1]Meteorite	ALL	ALL	ALL	LEO	ALL	ALL	EF	EF	EF	EF	EF	EF
Incl. Type	B2	B2	B	B1	B1	CTA	A	CTA	CTA	CTA	CTA	B2
Wt. (mg)	3.86	24.25	15.07	25.27	29.16	37.16	40.82	50.64	26.97	25.7	13.09	49.58
Na_2O	0.45	0.13	0.27	0.05	0.05	0.07	0.03	0.03	0.10	0.06	0.04	0.09
MgO	10.60	11.08	13.03	13.79	12.8	10.01	12.23	7.25	6.29	4.45	9.34	10.51
Al_2O_3	32.80	31.75	32.85	35.74	34.51	34.25	39.17	35.12	32.24	37.61	32.91	30.52
[2]SiO_2	19.62	28.37	27.93	29.59	28.51	24.26	24.40	22.64	25.02	21.03	23.26	26.97
CaO	33.9	26.3	23.1	18.7	21.3	28.3	21.7	32.9	34.0	34.6	32.6	29.9
TiO_2	1.44	1.90	1.84	1.91	2.54	2.34	1.46	1.47	1.99	1.92	1.00	1.58
V_2O_3	0.08	0.11	0.15	0.16	0.09	0.18	0.05	0.16	0.09	0.09	0.15	0.12
MnO (ppm)	136	27.2	55.8	9.94	27.9	25.2	100.7	42.6	17.2	20.9	32.8	15.4
Fe (ppm)	11089	3623	8318	605	2029	5806	9551	4354	2763	2372	6968	3153
CaO/Al_2O_3	1.034	0.828	0.703	0.523	0.617	0.826	0.554	0.937	1.055	0.920	0.991	0.980

[1] Meteorite names: ALL = Allende; LEO = Leoville; EF = Efremovka.
[2] SiO_2 determined by difference. CTA = compact Type A inclusion.

volume proportions in the inclusion. From the proportions of mineral phases and their densities (3.0 g-cm^{-3} for melilite, 3.3 for fassaite, 2.76 for anorthite, and 3.583 for spinel), an average density was calculated and used for the mixed phase component when converting volume proportions to weight proportions. From the average phase compositions and their weight proportions, bulk inclusion compositions were calculated. For Type B1 inclusions, bulk compositions and densities of cores and mantles were calculated separately, their volume proportions were determined petrographically, and converted to weight proportions. The core and mantle compositions were then combined, according to their weight proportions, to obtain the inclusion bulk compositions.

For the purposes of this paper, we assume that the CMAST components present in the alteration products were present in the inclusions before alteration and that any gains or losses are negligible. Therefore, our modal recombination technique includes secondary alteration products in the calculation of bulk compositions. This is quite reasonable, as we are not considering fine-grained inclusions or heavily altered Type As, so the primary phases account for the vast majority of each of the CMAST components present in CAIs.

3. RESULTS

3.1. INAA

For this study, we sampled large inclusions, and analyzed larger aliquots than has been typically done in the past in the hope that this would lead to more representative sampling. We obtained from 5 to 200 mg of homogenized powder from each inclusion and analyzed aliquots of 3.86 to 50.64 mg (average: 28.5). In contrast, most neutron activation analyses reported in the literature are based on less than 2 mg of material (even submg samples have been commonly used) which are not taken from larger samples of homogenized powders. Analytical results are given in Table 1. The abundances of the major elements and V_2O_3 are similar to those of previously analyzed coarse-grained inclusions (e.g., Sylvester et al., 1992; 1993). As might be expected, the compact Type A inclusions have higher CaO contents than all but one of the Type B inclusions, the Efremovka samples have low Na_2O contents, and there is a wide range of CaO/Al_2O_3 ratios.

Results are illustrated in Figure 1, where they are compared to a trajectory of bulk equilibrium condensate compositions stable in a solar gas at $P^{tot} = 10^{-5}$ bar within the temperature range of 1200–1400K. The literature data were obtained by defocused beam analysis (Wark, 1981; Wark and Lovering, 1982; Nazarov et al., 1982), modal recombination (Beckett, 1986; MacPherson and Davis, 1993) and INAA (Mao et al., 1990; Sylvester et al., 1992; 1993; Palme and Wlotzka, 1979). These are the data considered by Grossman et al. (2000), and, as in that work, are normalized to 100% CMAS. Figure 1a is a plot of CaO vs. Al_2O_3. Once these oxides are completely condensed, the CaO/Al_2O_3 ratio of the condensation trajectory remains fixed at the solar value, as it should for the hibonite-free inclusions considered here. As Figure 1a shows, neither the literature data nor the compositions of the relatively large samples analyzed for this study fall on the condensation trajectory. Instead of plotting on or along the trajectory, the data are spread out in an array that intersects the trajectory at a high angle, representing a wide range of mixtures of the constituent phases, especially in terms of the spinel/melilite (åkermanite-gehlenite series) ratio. This appears to be typical of refractory inclusion analyses. Wide ranges of CaO/Al_2O_3 ratios are also seen in the data of Conard (1976) and Mason and Martin (1977), for example. In both plots in Figure 1, the new data overlap the old. Although the new data form a somewhat tighter cluster about the condensation trajectory, analyzing samples that are larger by an order of magnitude has not resulted in a strong indication that true inclusion compositions match those of calculated equilibrium condensate assemblages.

Considering the CaO/Al_2O_3 ratios obtained, the results for a total of 29 refractory inclusions analyzed by INAA are illustrated in Figure 2a. Fifteen of the analyses are from the literature and were included in the study of Grossman et al. (2000), two are unpublished analyses from this laboratory, and the remaining 12 are the new analyses collected for the present study (Table 1). A wide range of CaO/Al_2O_3 ratios, from 0.52 to 1.38 is observed, with no suggestion of a gaussian distribution about the solar value. The average, 0.88, is within 1σ of the solar value, but $\sigma = 0.21$, or 24.0% of the average, so it is fairly large. Removal from consideration of very small samples ($\leq$2 mg), leaving only one inclusion from Grossman et al. (2000), eliminates the samples with the highest CaO/Al_2O_3 ratios. These probably oversampled melilite. This yields a suite of samples comprising 7 Type As with a mean ratio of 0.86 $\pm$ 0.17 and 8 Type Bs with a mean ratio of 0.75 $\pm$ 0.20. As

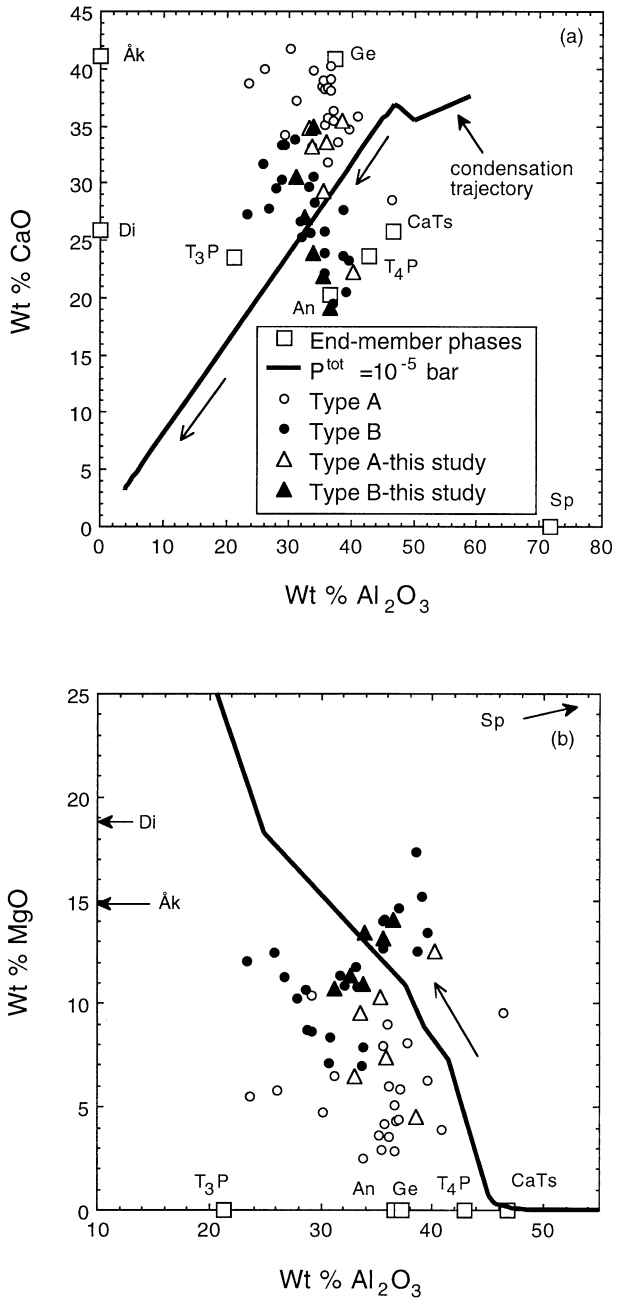

Fig. 1. Major element oxide concentrations in coarse-grained Types A and B refractory inclusions analyzed by INAA for this study (triangles) and the suite compiled by Grossman et al. (2000) (circles) compared to the composition trend of equilibrium condensate assemblages calculated to form from a solar gas at $P^{tot} = 10^{-5}$ bar at temperatures from 1200–1400K (Grossman et al., 2000). Unlabeled arrows indicate the direction of decreasing temperature along the condensation trend. (a) CaO vs. Al_2O_3. (b) MgO vs. Al_2O_3. Where possible, open squares indicate compositions of endmember components of the constituent phases of the inclusions: Åk = åkermanite; Ge = gehlenite; Di = diopside; CaTs = Ca-Tschermak's molecule; T_3P = $CaTi^{3+}SiAlO_6$ (pyroxene component); T_4P = $CaTi^{4+}Al_2O_6$ (pyroxene component); An = anorthite; Sp = spinel.

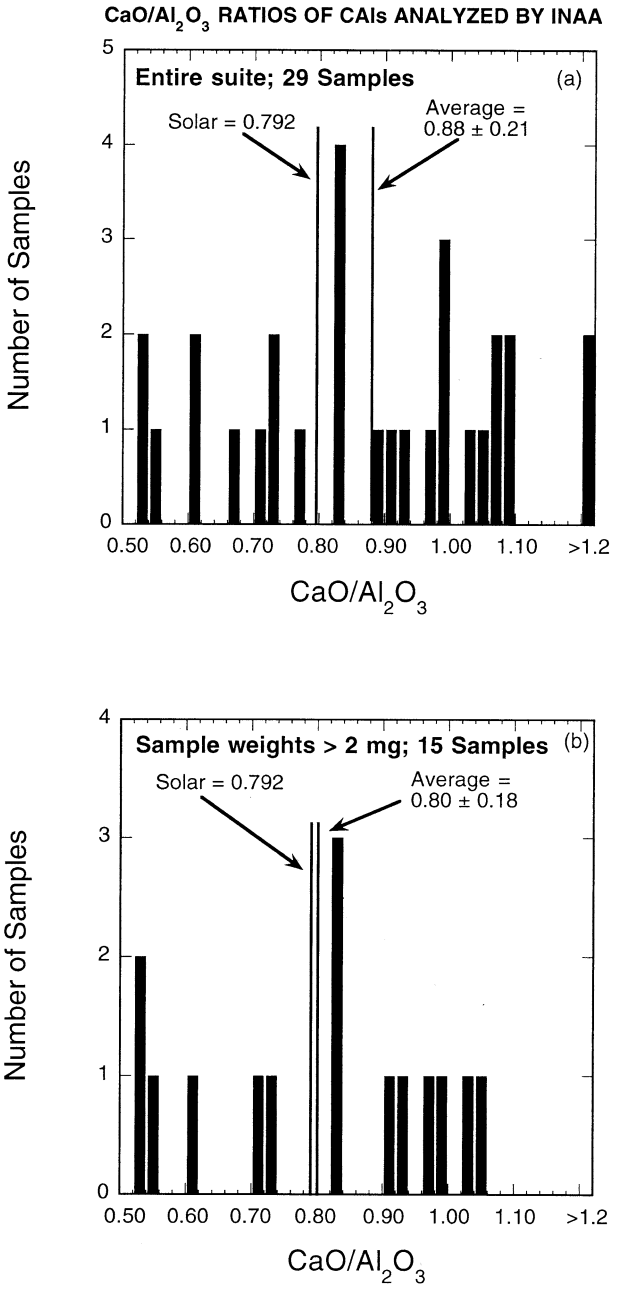

Fig. 2. Histograms of CaO/Al_2O_3 ratios of refractory inclusion samples analyzed by INAA. (a) A suite of 29 samples, with sizes ranging from 49.5 μg to 50.6 mg. The average ratio is higher than the solar value and the standard deviation is high. (b) Results for samples >2 mg. The average is close to the solar value but the standard deviation is still high.

illustrated in Figure 2b, the mean ratio of these 15 samples is 0.80, very close to the solar value, but with only a slightly smaller standard deviation, 0.18 (22.5%), than that of the entire suite including the small samples. This shows that when large (i.e., tens of mg) samples are analyzed by INAA, the average CaO/Al_2O_3 ratio becomes very close to the solar ratio, but analyses of individual inclusions still show considerable scatter about the mean. If each inclusion has the solar CaO/Al_2O_3 ratio, even analysis of ~40 mg from a homogenized powder weighing 56 mg does not assure representative sampling of refractory inclusions.

3.2. Modal Recombination

Another commonly used technique is modal recombination. As is the case when sampling for INAA, a thin section samples only a small portion of an inclusion and a random section may do so nonrepresentatively. This is especially likely in the case of compact Type A inclusions (CTAs) and Type B1 inclusions. The CTAs are almost completely composed of melilite + spinel, but the spinel is very heterogeneously distributed within these inclusions (Simon et al., 1999). It is thus quite unlikely that a random section will contain the specific melilite/spinel ratio that will yield the CaO/Al_2O_3 ratio of the whole inclusion. In the case of a Type B1 inclusion, the mantle will appear thicker than it should in an off-center section, and the diameter of the core will appear smaller than it should. In a rim-to-rim section, the degree to which it is off-center can only be estimated, if the entire inclusion is visible, by comparing the diameter of the inclusion observed in the section to that observed before sectioning. To evaluate the modal recombination technique, we compare our results for large and, in some cases multiple, sections of Type B inclusions to those of Beckett (1986), who analyzed one section from each of nine Type Bs. In that study, modes were obtained optically, and fine-grained regions were assumed to be secondary alteration products which, in turn, were assumed to have been melilite plus included phases originally.

The results of Beckett (1986) are illustrated in Figure 3a. Seven of the nine samples have CaO/Al_2O_3 ratios greater than the solar value, and there is a wide range of values, yielding a high standard deviation (24%). We analyzed 1 or 2 sections from each of eleven Type Bs, including some of the ones analyzed by Beckett (1986), and the results are illustrated in Figure 3b. The compositions are given in Table 2. As in the case for the INAA data, the new compositions obtained by modal recombination exhibit a great deal of overlap with the literature data while forming a tighter cluster about the condensation trajectory. The average CaO/Al_2O_3 ratio for our results, 0.79, is virtually identical to the solar ratio and is much closer to it than the average of the Beckett data (0.92). Our results have a narrower range than those of Beckett (1986) and the smallest standard deviation, 0.15 (19%), observed among the data sets summarized in Figures 2 and 3.

There are six thin sections that were analyzed both by us and by Beckett (1986). As in the results for the entire suites, among this subset our results tend to be closer to the solar value, with the Beckett data having a higher average CaO/Al_2O_3 ratio than our data, 0.92 ± 0.21 vs. 0.76 ± 0.17. To determine the reason for this, we carefully examined the results for two Type B2 inclusions in which our analysis of a thin section yielded a CaO/Al_2O_3 ratio within 10% of the solar value while Beckett (1986) determined a CaO/Al_2O_3 ratio >1 for the same section. We found that there are two likely causes for the systematic differences between our results and those of Beckett (1986). One is that the analyses by Beckett (1986) tend to have much higher modal abundances of secondary alteration products than are observed in the present work. This is probably because Beckett (1986) determined modal abundances optically and we did not. It can be seen with the SEM that heavily altered areas in these inclusions are not as extensive as they appear to be when viewed optically, so Beckett (1986) probably overestimated the amounts of secondary alteration products and added too much melilite plus included phases, a CaO-rich component, to his inclusion compositions. Our microbeam-based approach avoided that problem.

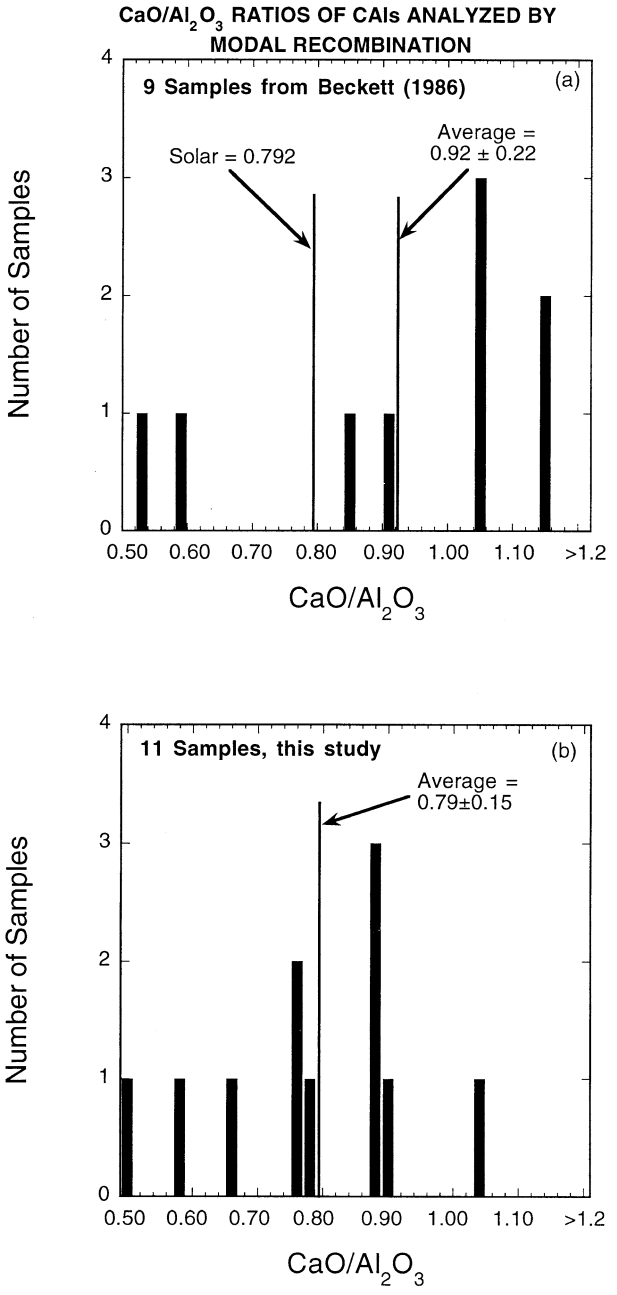

Fig. 3. Histograms of CaO/Al_2O_3 ratios of Type B refractory inclusions determined from thin sections by modal recombination. (a) Data from Beckett (1986), who used one section per inclusion. The average ratio is much higher than the solar value and the standard deviation is also high. (b) Data from this study, using 1 or 2 large, rim-to-rim sections of inclusions. The average ratio is almost identical to the solar ratio and the standard deviation is lower.

Secondly, if we ignore the alteration products, we find that our alteration-free inclusion compositions have lower CaO/Al_2O_3 ratios than those of Beckett (1986), reflecting another difference in the techniques used. In our calculations, we in-

Table 2. Bulk compositions of Type B inclusions, obtained by modal recombination and normalized to 100 wt% CMAST.

	E107		TS23		TS4		3537-2		TS33		TS65	TS67		Golfball		TS21		TS8		TS20	
	R	C	R	C	R	C	R	C	R	C	R	R	C	R	C	R	C	R	C	R	C
MgO	9.95	10.93	9.46	11.55	14.61	11.23	9.31	10.19	10.23	10.27	10.14	11.86	11.62	14.04	12.96	10.56	11.18	10.14	9.24	11.41	11.28
Al_2O_3	33.23	34.98	29.53	33.42	40.91	33.54	32.64	34.16	33.49	33.63	31.37	32.85	32.46	31.69	33.59	30.46	29.57	31.48	34.70	32.66	30.96	30.41
SiO_2	25.38	24.39	28.97	27.05	22.61	26.91	27.36	26.59	27.51	27.42	29.03	28.38	29.04	29.54	27.65	29.76	31.80	30.88	31.41	30.4	31.98	32.30
CaO	29.54	27.69	30.73	26.46	20.06	26.56	28.80	27.05	26.68	26.62	27.81	26.01	24.67	25.09	22.27	24.12	26.49	24.92	21.25	25.86	23.78	24.08
TiO_2	1.90	2.02	1.29	1.52	1.82	1.77	1.90	2.01	2.09	2.06	1.65	1.74	1.96	2.06	2.45	2.69	1.58	1.55	2.51	1.85	1.87	1.93
An/Ge		0.183		0.335		0.337		0.343		0.404		0.456		0.552		0.554		0.686		0.695		0.866
# Corr.		2		2		2		2		3		4		6		6		5		1		3

R: Raw, uncorrected data. C: Corrected to solar CaO/Al_2O_3 as described in the text. An and Ge components calculated using the method of Stolper (1982). # Corr.: number of corrections used in calculation of the average composition.

clude all analyses of contacts between different phases that have good analytical sums. Because spinel is fine-grained in these inclusions, many of these mixed-phase analyses have significant spinel components and low CaO/Al_2O_3 ratios. In contrast, when Beckett (1986) encountered a grain boundary during point-counting, he made an effort to classify the point as a single phase, and was able to do so for most of the points that hit contacts. Where he could not do so, a half-point was added to the modes of both of the phases in contact, but such cases were rare. Therefore the modal data of Beckett (1986) probably include fewer multigrain points than the present data, which, based on our results, tend to be Al_2O_3-rich. Classification of a contact as one phase or another does not lead to an accurate representation of the composition of that point in the calculation of the bulk composition of the inclusion; use of actual analyses is preferable. From the differences between the techniques used and resulting differences between alteration-free compositions obtained in the two studies, it appears that Beckett (1986) underestimated the spinel components of the inclusions. Both overestimation of secondary phase abundances and underestimation of spinel abundances will bias the results toward high CaO/Al_2O_3 ratios. From these findings we conclude that the method we used is more accurate than that of Beckett (1986), as are the relatively lower, near-solar CaO/Al_2O_3 ratios we obtained. None of our ratios for a given section are within 10% of the result obtained by Beckett (1986) for that section, but most are within ~15%, suggesting that this is the limit of agreement between the two techniques.

Somewhat better agreement is seen when we compare our results for two sections of the same inclusion. In two of the four cases where two sections of an inclusion were available, results agree to within ~2%, with one pair ~10% greater than the solar value and one pair ~16% below the solar value. In the other two cases, however, the results agree to within 15%. In one pair the samples have CaO/Al_2O_3 ratios 6 and 20% greater than the solar value, and in the remaining case, one section gave a subsolar value by 10% and the other section gave a CaO/Al_2O_3 ratio 2% greater than the solar value. With the same technique being used on both sections, this shows that sample heterogeneity alone can account for deviations of as much as $\pm$7.5% from the average CaO/Al_2O_3 ratio of an inclusion. This represents nearly half of the standard deviation about the solar value seen in our entire suite of modal recombination data (Fig. 3b).

Note that the data sets with the smallest standard deviations (Figs. 2b and 3b), albeit by small margins, both have average CaO/Al_2O_3 ratios that are much closer to the solar value than those of the data sets with larger standard deviations (Figs. 2a and 3a). Unless this is a fortuitous result, the data suggest that true inclusion bulk compositions do have the solar CaO/Al_2O_3 ratio. One way we can evaluate this conclusion is to look at the CaO/Al_2O_3 ratios in the six samples that were analyzed by both INAA and modal recombination (EMP) for this study (Table 3). The occurrence of samples in which both the modal recombination and the INAA results are much lower or much higher than the solar value would suggest true differences from solar. The data in Table 3 show that there are no such cases. For five of the six samples, the EMP value is within 15% of the solar value; in the one case where it is not, the INAA analysis is within

Table 3. CaO/Al_2O_3 ratios of samples analyzed by both modal recombination (EMP) and INAA.

Sample	EMP	Rel. Diff. (%)	INAA	Rel. Diff. (%)
TS67	0.761	−3.88	1.034	+30.56
TS65	0.887	+11.94	0.828	+4.55
Golfball	0.663	−16.29	0.703	−11.24
3537-2	0.882	+11.40	0.523	−33.97
TS33	0.797	+0.61	0.617	−22.10
E107	0.889	+12.25	0.980	+23.74
Avg. departure from solar ratio		9.39		21.02

Rel. Diff. (%): The relative difference between observed and solar (0.792) CaO/Al_2O_3 ratios; = (observed − solar) × 100/0.792. The average is based on the absolute values of the relative differences.

15%. These are fairly small departures given the likely contribution from sample heterogeneity. The EMP data more consistently approach the solar value than do the INAA data. Four of the six CaO/Al_2O_3 ratios obtained by INAA differ from the solar value by more than 20% while none of the EMP values differ by that much, and the average difference for the INAA data is more than twice that of the EMP data. Same-sample reproducibility for EMP-INAA pairs is worse than that for our EMP data vs. those of Beckett (1986) or for EMP data for multiple sections of an inclusion.

There are two cases, however, in which the CaO/Al_2O_3 ratios of both the EMP and INAA results differ in the same sense from the solar value by more than 10%. Both inclusions are petrographically unusual. Sample E107 appears to have been partially remelted, resulting in a very heterogeneous texture with regions that are either spinel-rich or nearly spinel-free, making it difficult to sample representatively, much like the case for compact Type A inclusions. As is commonly the case for CTAs, the analyses of E107 have CaO/Al_2O_3 ratios higher than the solar value. Those of Golfball, on the other hand, have low CaO/Al_2O_3 ratios. This inclusion has the unique feature of a melilite-rich core and a fassaite-rich rim (Simon et al., 2002b). Off-center sectioning of this inclusion could easily have occurred, which would lead to undersampling of melilite and to a low CaO/Al_2O_3 ratio.

In summary, using larger samples for INAA and an improved modal recombination technique compared to previous studies has yielded results in which the average CaO/Al_2O_3 ratios are identical to solar, with smaller standard deviations than previously observed. This is what we would expect with improved, but not perfect, sampling of a suite of inclusions in which each sample has the solar CaO/Al_2O_3 ratio. While we cannot rule out the possibility that each inclusion has a near-solar ratio and only the overall average has the solar value, the data suggest, and we will assume for the purposes of this paper, that the true bulk composition of each inclusion has exactly the solar CaO/Al_2O_3 ratio and that it is valid to correct our data for sample heterogeneity and for sampling errors. Our preferred method for doing so is described below.

3.3. Correction of Bulk Compositions to the Solar CaO/Al_2O_3 Ratio

Although Grossman et al. (2000) found that correcting inclusion compositions to the solar CaO/Al_2O_3 ratio by addition or subtraction of spinel greatly reduced scatter and improved fits of the data to condensation trajectories, if one mineral is over- or undersampled, something else may be missampled as well. This one-phase correction is sufficient for Type As, however, because they mainly consist of melilite + spinel, so adding one is equivalent to subtracting the other. But, for Type Bs, fassaite and anorthite can be sampled nonrepresentatively in addition to melilite and spinel. Adding or subtracting only one phase is unlikely to account for all sampling errors in Type Bs, because in each single-phase correction calculation, the relative proportions of the other phases remain constant.

In the preliminary report of this work (Simon et al., 2002a), we added melilite and fassaite corrections to our bulk composition calculations. Simon et al. (2002a) did not include a correction for anorthite, based on the assumption that it is present in only minor amounts in most Type B inclusions and therefore gross under- or oversampling of it would only have a minor effect upon the calculated bulk composition. After calculations showed that the more SiO_2-rich Type B2s could contain up to ~20 wt.% anorthite, we tested an anorthite correction calculation. This worked only for the two compositions that required very small corrections, however. Anorthite has neither an extremely high CaO/Al_2O_3 ratio with a high CaO content like melilite, nor a high Al_2O_3 content with an extremely low CaO/Al_2O_3 ratio as does spinel. In contrast, the CaO and Al_2O_3 contents of anorthite and its CaO/Al_2O_3 ratio are relatively close to those of uncorrected inclusion compositions so that, in many cases, corrections require large additions or subtractions of the anorthite component. Considering the lack of MgO and TiO_2 in anorthite, such corrections yield absurd inclusion compositions, e.g., 34.1 wt.% MgO, 3.5 wt.% SiO_2 and 8.4 wt.% TiO_2 in a Type B2 inclusion from which anorthite was subtracted to give the solar CaO/Al_2O_3 ratio. We concluded that three corrections are sufficient, have expanded the correction technique of Grossman et al. (2000) to include fassaite and melilite in addition to spinel, and applied it to our modal recombination results for Type B inclusions.

The procedure is as follows. First, electron probe traverses are conducted across an inclusion, and a bulk composition is calculated as described in the Experimental Methods section. The individual analyses, average phase compositions, and the raw calculated bulk compositions are plotted, and the triangle defined by the average spinel, fassaite, and melilite compositions used in the correction is drawn, as in the example shown in Figure 4. Anorthite plots within the triangle. Most analyses either plot at the compositions of the major phases or grossular, or are dispersed along mixing lines between them. Monticellite-dominated analyses plot outside the triangle and outside the range of melilite-fassaite mixtures. Two bulk compositions are plotted because we analyzed two thin sections of this inclusion.

Next, spinel-, fassaite-, and melilite-corrected bulk compositions are calculated from each, and a total of six corrected compositions are plotted in Figure 4. The correction procedure constrains them to fall on a line whose slope is the solar CaO/Al_2O_3 ratio. The average of the corrected compositions

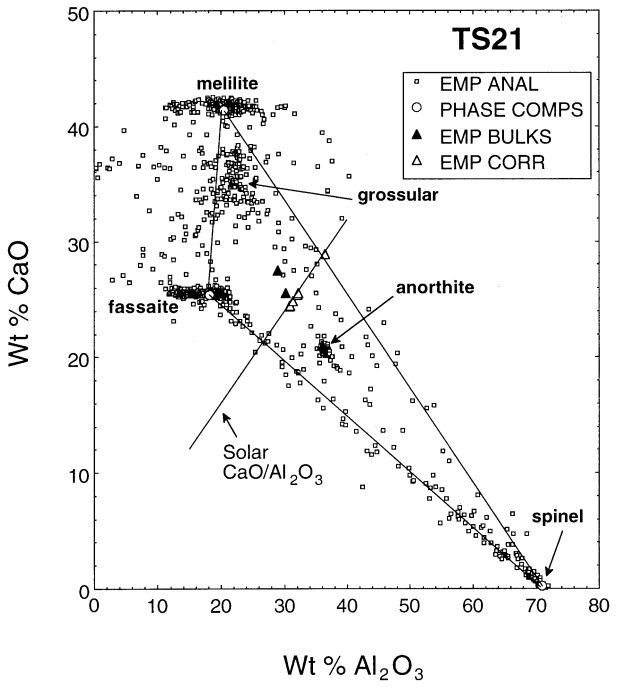

Fig. 4. Example of a plot used in correction of raw modal recombination results to compositions with the solar CaO/Al_2O_3 ratio, showing individual electron probe analyses ("EMP analyses"), average phase compositions, raw bulk compositions ("EMP Bulks"), and corrected bulk compositions ("EMP Corrected"), which have solar CaO/Al_2O_3, for two sections of Allende Type B2 inclusion TS21. One correction, reflecting fassaite subtraction, plots outside the triangle and represents a composition with a negative fassaite component, so it would not be included in the calculation of an average corrected composition.

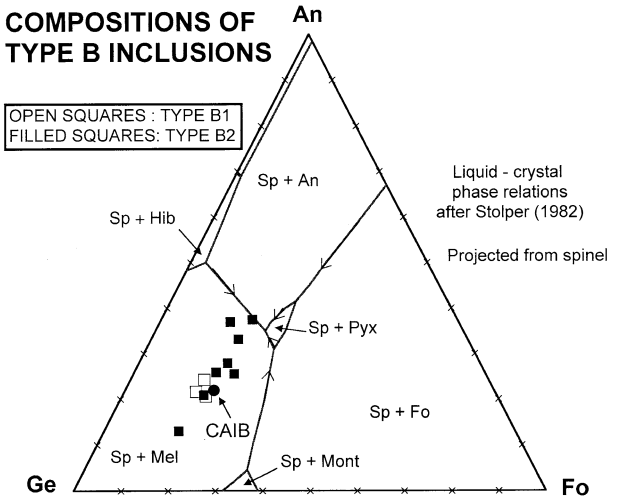

Fig. 5. Projection of average corrected bulk compositions of Type B inclusions from spinel (Sp) onto the gehlenite (Ge)-anorthite (An)-forsterite (Fo) plane in the CMAS system. Type B2s tend to have higher An/Ge component ratios than B1s. CAIB = average Type B composition of Stolper (1982); Hib = hibonite; Pyx = clinopyroxene; Mont = monticellite.

gives an average corrected composition for the inclusion. In Figure 4, one of the individual corrected compositions plots close to the melilite-spinel join, just outside the three-phase triangle. This point corresponds to an assemblage with negative fassaite (and negative TiO_2), an impossible result. This particular corrected composition was obtained by subtracting fassaite from the raw bulk composition, in essence assuming that the section that was studied oversampled fassaite. Apparently, this cannot be the cause of the non-solar CaO/Al_2O_3 ratio in the raw data, so this corrected composition was not included in the calculation of the average corrected bulk composition of this inclusion. Instead, the raw compositions probably undersampled spinel and oversampled melilite.

The case illustrated in Figure 4 is fairly typical, as the fassaite correction was rejected in eight of fifteen calculations. For six of the sections it gave negative or zero TiO_2, and in two cases the bulk TiO_2 and fassaite contents were much higher than are observed in Type B CAIs and would correspond to $>$65 wt.% fassaite. The melilite correction was accepted in all cases, and the spinel correction was used in all but one case.

The average of the corrected compositions for each inclusion, by accounting for under- and oversampling of all major phases, is the best estimate of the true bulk composition of that inclusion. The average corrected bulk compositions obtained in this way for our suite of Type B inclusions are given in Table 2, and are plotted in Figure 5 along with CAIB, the average Type B composition used by Stolper (1982).

Spinel is the first phase to crystallize from liquids of these compositions. The data are projected from spinel onto the gehlenite (Ge)-forsterite (Fo)-anorthite (An) plane in the CMAS system. All plot in the Sp + Mel field, so for these compositions, melilite follows spinel in the equilibrium crystallization sequence. The three Type B1s (TS23, 3537-2, TS33) plot very close to each other and to CAIB but six of the other eight inclusions plot between the B1s and the melilite-anorthite field boundary. As this plot shows, CAIB is representative of Type B1 compositions, but B2s have a wide range of normative An/Ge component ratios, from 0.183 to 0.866 (Table 2), most of which are higher than those of B1s and are not properly represented by a single composition. The inclusion with the largest Ge component is E107, from Efremovka. It has an anomalously low normative An/Ge ratio for a Type B inclusion, especially a B2. Its bulk composition is more like that of a Type B1 inclusion than a B2. The thin section shows that it is indeed very melilite-rich, with pockets of fassaite, anorthite and spinel enclosed in melilite. Based on its texture, it has probably been remelted, so it could have originally had the texture of a B1, but since it has Type B mineralogy and does not have a pyroxene-rich core enclosed by a melilite mantle, it must be classified as a B2. Compositions of Type A inclusions plot much closer to the Ge apex than does E107.

4. DISCUSSION

4.1. Effects of Variation of the Normative An/Ge Ratio in Type B Inclusions

The range in normative An/Ge ratios reflects variations in the bulk compositions that have implications for the petrographic features of the inclusions. We used the Berman (1983) CMAS activity model to calculate the compositions and incoming temperatures of the first melilite expected to crystallize in each of the inclusions we studied. These results are summarized in

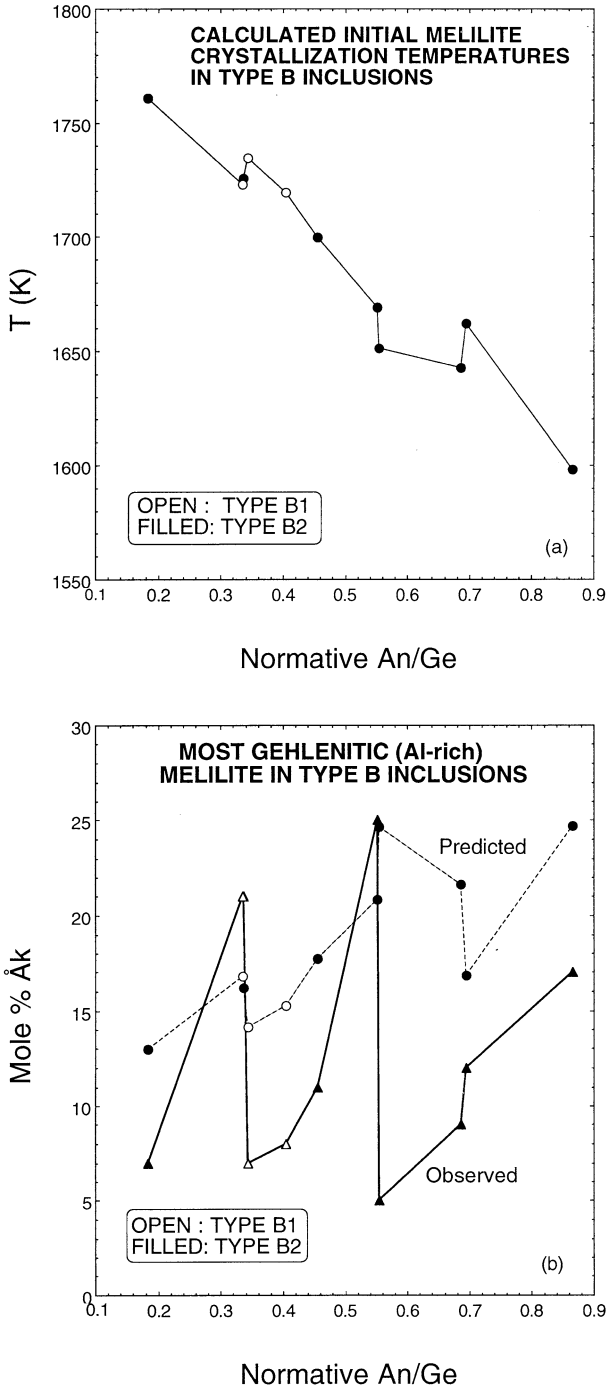

Fig. 6. (a) Calculated temperature of the onset of melilite crystallization as a function of normative An/Ge ratio. Melilite should begin crystallizing at lower temperatures in typical Type B2s than in B1s. (b) Predicted and observed compositions of the most gehlenitic melilite in Type B inclusions as a function of the normative An/Ge ratio. The agreement is not good, at least partially due to the presence of relict gehlenitic grains in the inclusions.

Figure 6. With increasing normative An/Ge, the predicted melilite incoming temperatures generally decrease, from 1760K in E107 to 1598K in TS20 (Fig. 6a). This is in qualitative agreement with the phase diagram, which predicts decreasing temperature intervals of spinel + melilite crystallization, and less prior crystallization before incoming of fassaite, with increasing normative An/Ge. This can affect the morphology, compositions, and zoning of melilite and fassaite, and knowing this can help us understand some of the differences between B1s and B2s, because B2s tend to have higher normative An/Ge ratios than B1s. For example, the thick melilite mantles in B1s may be a consequence of the wider temperature intervals of melilite crystallization before incoming of pyroxene and anorthite in B1s than in B2s.

As the Ge component in the inclusion bulk compositions decreases, the composition of the initial melilite to crystallize also changes. As illustrated in Figure 6b, with increasing An/Ge the åkermanite content of the first melilite is predicted to increase from 13 to 25 mol.% in these inclusions. The observed minimum åkermanite contents do not match the predicted values; in most cases, melilite more gehlenitic than expected is found. This is at least partially due to the presence of gehlenitic relict grains in these inclusions and limitations of the thermodynamic model.

Assuming that each inclusion originally consisted of the four primary phases with the average compositions that we measured and that alteration redistributed the major elements but did not cause a net gain or loss of any of the CMAST oxides, we calculated the primary mineral proportions that correspond to each of the corrected bulk compositions. These are shown in Figure 7, with the phase abundances plotted in wt.%. With increasing normative An/Ge, the proportion of melilite decreases, by up to ~25 wt.%, and it becomes more åkermanitic (Fig. 7a). The melilite is largely replaced by anorthite; fassaite increases only slightly, and spinel decreases slightly with increasing An/Ge (Fig. 7b). Type A inclusions have lower An/Ge ratios than Type B inclusions. Extrapolation of the observed trends to lower An/Ge leads to the prediction of very high contents of relatively gehlenitic melilite, which is observed in both the fluffy (MacPherson and Grossman, 1984) and compact (Simon et al., 1999) Type As.

4.2. Bulk Compositions and Implications for Thermal Histories

Grossman et al. (2000) used plots of SiO_2 vs. MgO to illustrate the offset of inclusion bulk compositions from the trajectory of equilibrium condensate compositions formed from a solar gas at $P^{tot} = 1 \times 10^{-5}$ bar, and we do so here (Fig. 8) for our average corrected Type B bulk compositions (Table 2) along with the spinel-corrected Grossman et al. (2000) suite. Error bars are shown for our data where they are larger than the symbol, and they represent the ranges of the corrected compositions used to obtain each point. The ranges are quite narrow in many cases, especially for MgO. We again find that the compositions are depleted in MgO and SiO_2 relative to the calculated bulk compositions of equilibrium condensate assemblages.

Our data overlap some of the previous analyses of Type Bs but the scatter among the Type Bs is greatly reduced, as is the range of implied losses by evaporation into an H_2-rich gas. Comparison of our results with contours of evaporative losses from Grossman et al. (2000), which are also shown in Figure 8, indicate that the bulk compositions of most Type B refractory

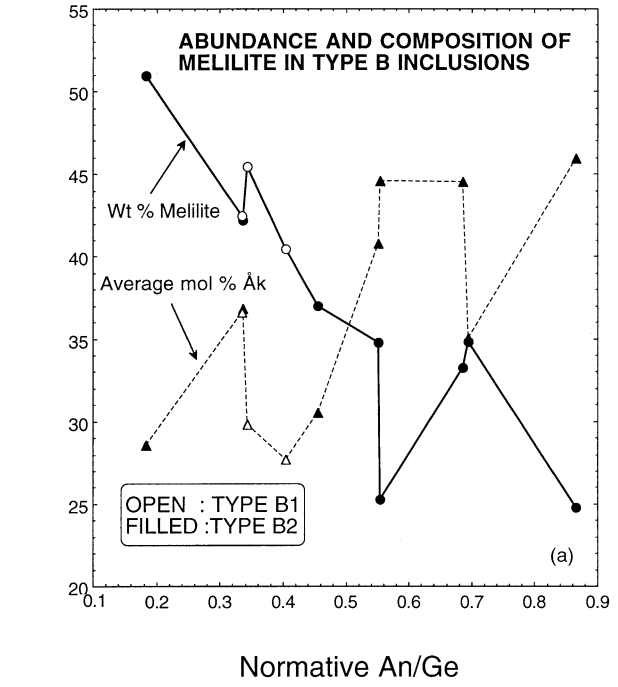

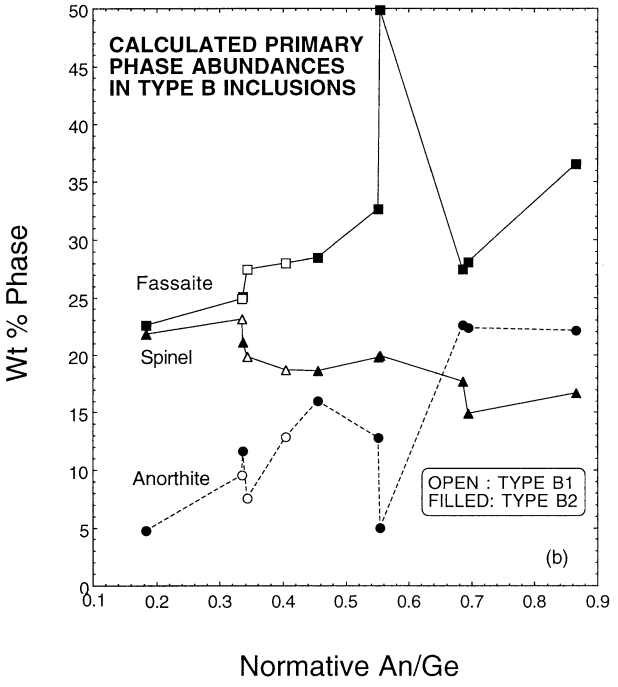

Fig. 7. Phase abundances calculated from the Type B inclusion bulk compositions, assuming the inclusions consist of only the four primary phases, as a function of normative An/Ge ratio. (a) Calculated melilite abundances and observed average compositions. Melilite abundances decrease and åkermanite contents increase with increasing An/Ge. (b) Calculated abundances of fassaite, spinel and anorthite. Melilite is mostly replaced by anorthite with increasing An/Ge, while spinel decreases slightly and fassaite increases slightly.

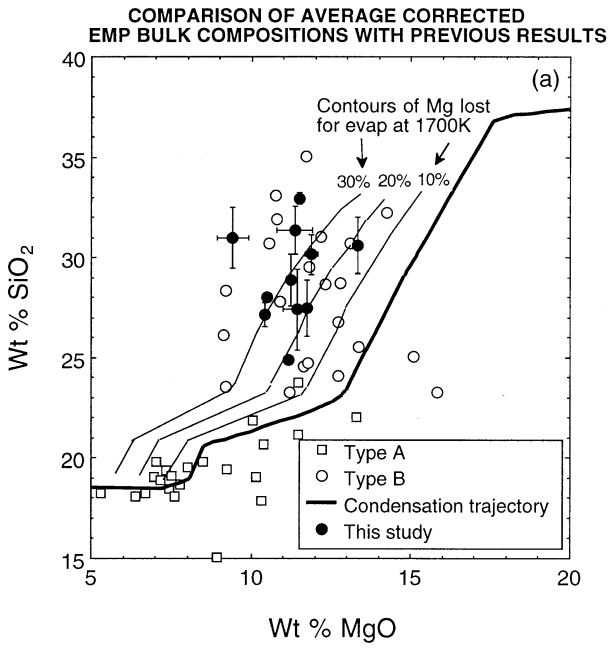

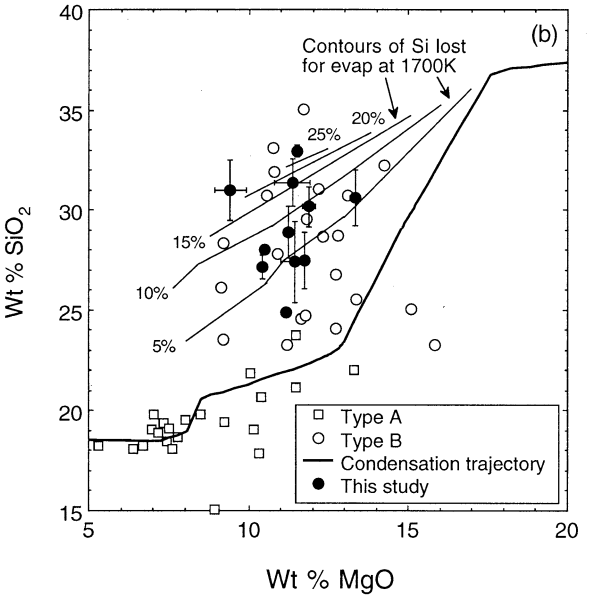

Fig. 8. Corrected bulk compositions of refractory inclusions compared to a trajectory of compositions of equilibrium condensate assemblages and contours of (a) Mg and (b) Si evaporative loss from those compositions. Most of the compositions of Type B inclusions obtained in the present study (Table 2) indicate evaporative losses of ~20–30% of the initial Mg and ~5–15% of the initial Si. The open symbols represent data from Grossman et al. (2000). Evaporative loss contours and the condensation trajectory (solar gas at 10^{-5} bar) are also from Grossman et al. (2000). All analyses are normalized to 100% CaO + MgO + Al_2O_3 + SiO_2 (CMAS).

inclusions could have been derived from bulk equilibrium condensate assemblages expected under the assumed physical conditions by simultaneous evaporative loss of ~20–30% of the original MgO and ~5–15% of the original SiO_2. These amounts of evaporation are within the ranges of those indicated by the bulk Mg and Si isotopic compositions of inclusions that

are available in the literature (Grossman et al., 2000). Representative paths of evaporation from this condensation trajectory into the field of CAI compositions are shown in Grossman et al. (2002). Note that very SiO_2-rich compositions and low-SiO_2, high-MgO compositions that are not readily explained by evaporative loss from equilibrium condensates are not observed in the new data shown here. The data from this study form a tighter cluster than the suite of data that Grossman et al. (2000) obtained from the literature, and this cluster falls in a significant place.

Grossman et al. (2000) modeled simple evaporation in pure H_2 from a variety of CMAS liquids having the solar CaO/Al_2O_3 ratio, without including crystallization effects. The more SiO_2-rich the starting composition, the more readily SiO_2 is lost from the melt relative to MgO (see Fig. 9 of Grossman et al., 2000). The same is true for MgO relative to SiO_2, so that most paths converge to a "main stream" of nearly constant slope on a plot of SiO_2 vs. MgO. This effect is shown for evaporation at 1800K and $P_{H_2} = 10^{-8}$ bar in Figure 9a. A wide variety of starting compositions, with solar CaO/Al_2O_3, 15–50 wt.% SiO_2 and 30–60 wt.% MgO, were modeled in decrements of 0.01 mol Mg in the liquid. No losses of CaO or Al_2O_3 were indicated by the calculations. Despite the wide range of starting compositions, most of the evaporation paths converge to a single trend below ~15 wt.% MgO. The position of the main stream varies with the temperature of evaporation. In Figure 9b, in addition to the 1800K path, the trends for evaporation at 1700K and 2000K and $P_{H2} = 10^{-8}$ bar are represented by single lines. Note that the SiO_2/MgO ratios of the trends increase with decreasing evaporation temperature. The cluster of inclusion compositions obtained in this study lies astride the main stream for 1800K, and is bracketed by the 1700K and 2000K paths.

These results clearly show that, although the bulk chemical compositions of many coarse-grained refractory inclusions are consistent with evaporative losses of 20–30% of the original Mg and 5–15% of the original Si from equilibrium condensate assemblages that define one particular trajectory, there are numerous histories that could have yielded these compositions. As illustrated in Figure 9a, many different paths, from many different starting compositions, can lead to the observed inclusion bulk compositions, but after very different amounts of evaporative losses of Mg and/or Si. As shown in Figure 9b and by Grossman et al. (2000), the amount of SiO_2 lost relative to the amount of MgO lost varies with the temperature of evaporation. Thus, many different combinations of Mg and Si loss are possible. Measurement of the bulk Mg, Si and O isotopic compositions of these inclusions, which is currently being undertaken, in combination with their bulk compositions, should constrain their initial bulk compositions and the paths the inclusions followed to their final compositions. This will allow determination of how closely the original compositions of the inclusions match those of equilibrium condensate assemblages. This will be a major step forward in our understanding of the formation of coarse-grained refractory inclusions.

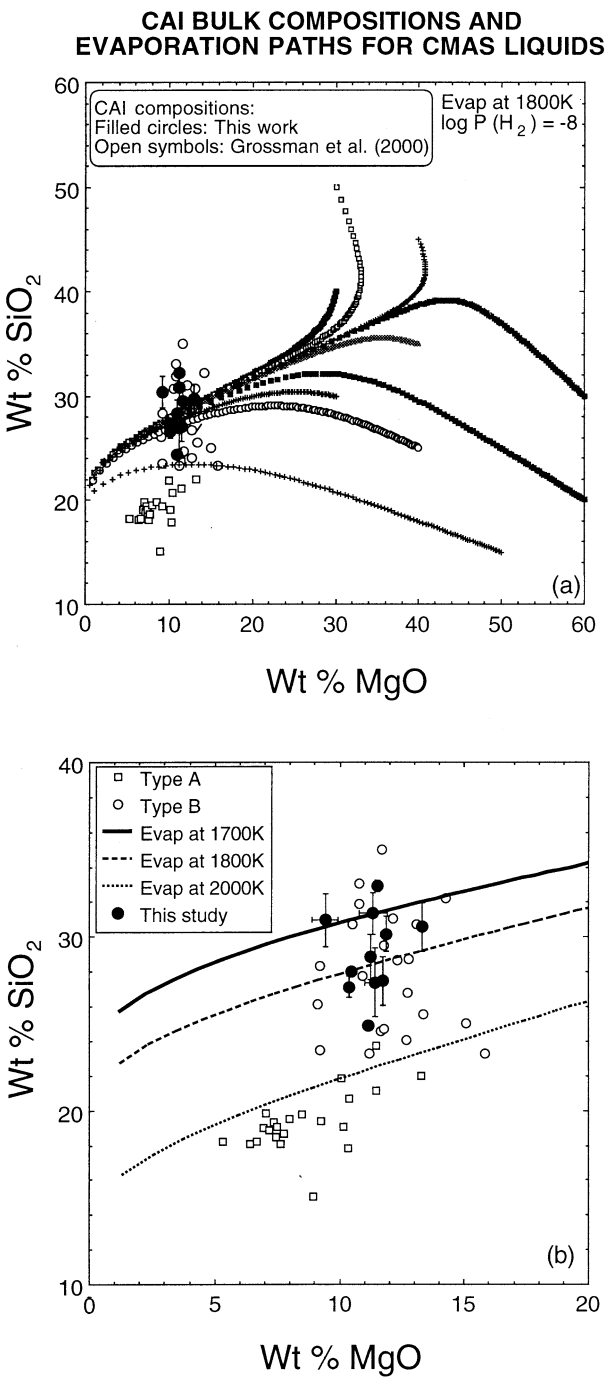

Fig. 9. Corrected bulk compositions of refractory inclusions compared to evaporation paths of CMAS liquids. (a) Evaporation of many different starting compositions at 1800K. The analyses of Type B inclusions from the present study (Table 2) straddle the main stream of evaporation paths. (b) Representation of main streams of evaporation paths at 1700, 1800, and 2000K, which bracket the compositions obtained in the present study. The open symbols represent data from Grossman et al. (2000). All analyses are normalized to 100% (CMAS).

5. CONCLUSIONS

Bulk analyses of coarse-grained CAIs found in the literature typically do not have the solar CaO/Al_2O_3 ratio. Analysis of large aliquots by INAA, or modal recombination of thin sections with cross-sections of entire, unbroken CAIs, however, yields bulk compositions whose average CaO/Al_2O_3 ratio is the solar value, with smaller standard deviations about this value

than previously observed. Because this is what we would expect with improved sampling of a suite of inclusions in which the true bulk composition of each sample has the solar CaO/Al_2O_3 ratio, the data suggest that this is the case. Assuming this is true, a bulk analysis of an inclusion can be corrected to the solar CaO/Al_2O_3 ratio by mathematical addition or subtraction of melilite, spinel, or fassaite of the average composition observed in the inclusion. This yields multiple, potential corrected compositions for a given inclusion. Because these individual corrections are based on the addition or subtraction of one phase while holding the relative proportions of all other phases constant, the best estimate of the bulk composition of an inclusion is the average of its corrected compositions.

Results show that Type B2 inclusions exhibit a wide range of normative Anorthite/Gehlenite component ratios and generally have higher SiO_2 contents than Type B1 inclusions. The average corrected bulk compositions of the suite of Type B inclusions studied here tend to cluster along trends generated by evaporation (at 1700–2000K and $P_{H_2} = 10^{-8}$ bar) of CMAS liquids with solar CaO/Al_2O_3, initial MgO contents of 30–60 wt.% and initial SiO_2 contents of 15–50 wt.%. Determination of the bulk isotopic compositions of these inclusions will allow estimation of the degrees of evaporation they underwent. From that information their original compositions can be determined to see whether or not they match those of equilibrium condensate assemblages.

Acknowledgments—We wish to thank A. N. Krot and A. A. Ulyanov for kindly sharing samples and images of CAIs from Efremovka, D. S. Ebel for performing the condensation and evaporation calculations, and A. Fedkin for helpful thermodynamic calculations related to melilite stability. Samples were irradiated and counted by M. Glascock, who also reduced the INAA data. Comments from H. Connolly, Y. Lin, D. Mittlefehldt and an anonymous reviewer led to improvements in the text. This work was supported by the National Aeronautics and Space Administration through grant NAG5-11588 and funding is gratefully acknowledged.

Associate editor: D. Mittlefehldt

REFERENCES

Amelin Y., Grossman L., Krot A. N., Pestaj T., Simon S. B., Ulyanov A. A. (2002) U-Pb age of refractory inclusions from the CV carbonaceous chondrites Allende and Efremovka. *Lunar Planet. Sci. XXXIII*. Lunar Planet. Inst., Houston. #1151 (abstr.).

Anders E. and Grevesse N. (1989) Abundances of the elements: Meteoritic and solar. *Geochim. Cosmochim. Acta* **53,** 197–214.

Beckett J. R. (1986) The origin of calcium-, aluminum-rich inclusions from carbonaceous chondrites: an experimental study. Ph.D. thesis, Univ. Chicago.

Berman R. G. (1983) A thermodynamic model for multicomponent melts, with application to the system $CaO-MgO-Al_2O_3-SiO_2$. Ph.D. thesis, Univ. Br. Columbia.

Clayton R. N., Hinton R. W. and Davis A. M. (1988) Isotopic variations in the rock-forming elements in meteorites. *Phil. Trans. R. Soc. Lond.* **A325,** 483–501.

Conard R. (1976) A study of the chemical composition of Ca-Al-rich inclusions from the Allende meteorite. M.S. thesis. Oregon State Univ.

Dowty E. and Clark J. R. (1973) Crystal structure refinement and optical properties of a Ti^{3+} fassaite from the Allende meteorite. *Am. Min.* **58,** 230–242.

Glascock M. D., Tian W. Z. and Ehmann W. D. (1985) Utilization of a boron irradiation vessel for NAA of short-lived radionuclides in biological and geological materials. *J. Radioanal. Nuc. Chem.* **92,** 379–390.

Grossman L. (1972) Condensation in the primitive solar nebula. *Geochim. Cosmochim. Acta* **36,** 597–619.

Grossman L., Ebel D. S., Simon S. B., Davis A. M., Richter F. M. and Parsad N. M. (2000) Major element chemical and isotopic compositions of refractory inclusions in C3 chondrites: The separate roles of condensation and evaporation. *Geochim. Cosmochim. Acta* **64,** 2879–2894.

Grossman L., Ebel D. S. and Simon S. B. (2002) Formation of refractory inclusions by evaporation of condensate precursors. *Geochim. Cosmochim. Acta* **66,** 145–161.

Lin Y. and Kimura M. (2003) Ca-Al-rich inclusions from the Ningqiang meteorite: Continuous assemblages of nebular condensates and genetic link to Type B inclusions. *Geochim. Cosmochim. Acta* **67,** 2251–2267.

MacPherson G. J. and Davis A. M. (1993) A petrologic and ion probe study of a Vigarano Type B refractory inclusion: Evolution by multiple stages of alteration and melting. *Geochim. Cosmochim. Acta* **57,** 231–243.

MacPherson G. J. and Grossman L. (1984) "Fluffy" Type A Ca-, Al-rich inclusions in the Allende meteorite. *Geochim. Cosmochim. Acta* **48,** 29–46.

Mao X.-Y., Ward B. J., Grossman L. and MacPherson G. J. (1990) Chemical compositions of refractory inclusions from the Vigarano and Leoville carbonaceous chondrites. *Geochim. Cosmochim. Acta* **54,** 2121–2132.

Mason B. and Martin P. M. (1977) Geochemical differences among components of the Allende meteorite. *Smithson. Contrib. Earth Sci.* **19,** 84–95.

Nazarov M. A., Ulyanov A. A., Korina M. I. and Kolesov G. M. (1982) Efremovka CAI's: Major and trace element chemistry. *Lunar Planet. Sci. XIII,* 584–585(abstr.).

Niederer F. R. and Papanastassiou D. A. (1984) Ca isotopes in refractory inclusions. *Geochim. Cosmochim. Acta* **48,** 1279–1293.

Palme H. and Wlotzka F. (1979) A Ca, Al-rich inclusion from the Leoville (C3V)-meteorite. *Meteoritics* **14,** 508–511. (abstr.).

Pouchou J. L. and Pichoir F. (1984) A new model for quantitative x-ray microanalysis. Part I: Application to the analysis of homogeneous samples. *Rech. Aerosp.* **1984–3,** 13–38.

Simon S. B., Davis A. M. and Grossman L. (1999) Origin of compact Type A refractory inclusions from CV3 carbonaceous chondrites. *Geochim. Cosmochim. Acta* **63,** 1233–1248.

Simon S. B., Grossman L., Krot A. N., Ulyanov A. A. (2002a) Bulk chemical compositions of Type B refractory inclusions. *Lunar Planet. Sci. XXXIII.* Lunar Planet. Inst., Houston. #1620 (abstr.).

Simon S. B., Davis A. M. and Grossman L. (2002b) Golfball, a large Allende Type B inclusion with evidence for multiple stages of remelting. *Meteorit. Planet. Sci.* **37**(**suppl.**),A130 (abstr.).

Stolper E. (1982) Crystallization sequences of Ca-Al-rich inclusions from Allende: An experimental study. *Geochim. Cosmochim. Acta* **46,** 2159–2180.

Stolper E. and Paque J. M. (1986) Crystallization sequences of Ca-Al-rich inclusions from Allende: The effects of cooling rate and maximum temperature. *Geochim. Cosmochim. Acta* **50,** 1785–1806.

Sylvester P. J., Grossman L. and MacPherson G. J. (1992) Refractory inclusions with unusual chemical compositions from the Vigarano carbonaceous chondrite. *Geochim. Cosmochim. Acta* **56,** 1343–1363.

Sylvester P. J., Simon S. B. and Grossman L. (1993) Refractory inclusions from Leoville, Efremovka, and Vigarano C3V chondrites: Major element differences between Types A and B, and extraordinary refractory siderophile element compositions. *Geochim. Cosmochim. Acta* **57,** 3763–3784.

Wark D. A. (1981) The pre-alteration compositions of Allende Ca-Al-rich condensates. *Lunar Planet. Sci. XII,* 1148–1150(abstr.).

Wark D. A. and Lovering J. F. (1982) The nature and origin of type B1 and B2 Ca-Al-rich inclusions in the Allende meteorite. *Geochim. Cosmochim. Acta* **46,** 2581–2594.

Yoneda S. and Grossman L. (1995) Condensation of $CaO-MgO-Al_2O_3-SiO_2$ liquids from cosmic gases. *Geochim. Cosmochim. Acta* **59,** 3413–3444.